ACS APPLIED ELECTRONIC MATERIALS

pubs.acs.org/acsaelm Article

Ink-Coated Silver Films on PET for Flexible, High Performance Electromagnetic Interference Shielding and Joule Heating

Mingxuan Li, Sneh Sinha, Sima Hannani, S. Brett Walker, Melbs LeMieux, and Paul W. Leu*

Cite This: https://doi.org/10.1021/acsaelm.2c01183 Read Online

ACCESS | Metrics & More | Article Recommendations | Supporting Information

ABSTRACT: There is a need for high efficiency electromagnetic interference (EMI) shielding and highly efficient joule heating materials that may be incorporated into flexible substrates. In this work, we demonstrate silver films on polyethylene terephthalate (PET) with a low sheet resistance of 57 mohm/sq, high EMI shielding efficiency of 82.6 dB in the X band (8−12 GHz) and 85.3 dB in the Ku band (12−18 GHz), and high Joule heating performance with a stable temperature of 147.0 °C at only 1.5 V DC power input. The silver films are fabricated using a reactive particle free silver ink, which is cured at only 100 °C, and polyurethane diol (PUD) is utilized to enhance adhesion to PET. The PUD enables excellent mechanical flexibility, where the EMI shielding efficiency does not degrade after 10 000 times bending at a 0.4 cm bending radius. This work achieves high EMI SE with small film thickness of only 11.7 μm and stable high temperatures at low applied voltage, both of which have been difficult to achieve. This work demonstrates coated silver thin films on PET as a a flexible material for efficient EMI shielding protection and Joule heating that may be used for smart wearable devices, personal medical electronics, and next generation communications.

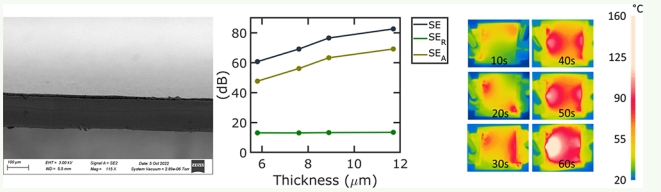

KEYWORDS: *EMI shielding, metal ink, flexible electronics, Joule heating, additive manufacturing*

INTRODUCTION

There is great interest in new electromagnetic interference (EMI) shielding materials with high shielding efficiency (SE) and flexibility. This need has grown rapidly recently due to the rise of 5G communication and personal electronics.[1] EMI shielding materials are needed to protect electronic devices from EM waves in the surrounding environment to keep devices working properly and accurately.[2,3] EMI shielding may also provide security to protect sensitive information[4,5] or ensure that electronic systems can withstand electromagnetic pulse weapons or attacks that could disable electronic systems.[6,7]

Traditional EMI shielding consists of metal cages, foils, and meshes.[8−10] However, these materials are thick, heavy, bulky, and rigid and are unsuitable for flexible electronics and wearables.[11] Conventional EMI shielding is fabricated by subtractive manufacturing methods such as die cutting, extrusion, or molding, which consume much material and energy and their cost is high.[12,13] New lightweight EMI shielding materials are needed that may accommodate a variety of substrates including polyethylene terephthalate (PET) for flexible electronics[14] or textiles for wearable electronics.[15,16]

It is important to achieve high SE with small thicknesses, as larger thickness films tend to more easily debond, crack, and tear during bending.[15] The bending stiffness of a film is proportional to the cube of its thickness[17] and thus, thinner materials are more desirable for flexible electronics.[18] For military defense applications, the requirement for SE is higher than 80 dB.[19,20] However, there has been difficulty in achieving shielding efficiency (SE) higher than 80 dB using materials with thickness smaller than 15 μm. This has included much research into novel materials such as carbon-based nanomaterials, MXenes, metal nanowires, and curable metals inks. 3D graphene with Ni nanoparticles has achieved 79 dB SE, but with a thickness of 327 μm.[21] Hyo-Jun et al. reported that plasma reduced Ag films could achieve 57.5 dB SE at thicknesses of 1.8 μm.[18] MXenes on polyester have been demonstrated to have 90 dB SE, but at a thickness of 1.3 mm.[22] Ag nanowires on cellulose are reported to have 101 dB SE at a thickness of 48.5 μm.[23] New materials that can achieve high SE at small thicknesses are needed for flexible EMI shielding.

Joule heating is widely used in heat management devices, especially for medical use.[22,24,25] According to Joule's law, higher voltage or lower resistance is required to increase heating power. It is preferred to utilize lower voltages in medical devices, as lower voltages are safer. It is reported that boron nitride nanosheet/aramid nanofibers-silver nanowires/aramid nanofibers achieve a stable temperature of 174.5 °C at

Received: September 7, 2022
Accepted: December 7, 2022

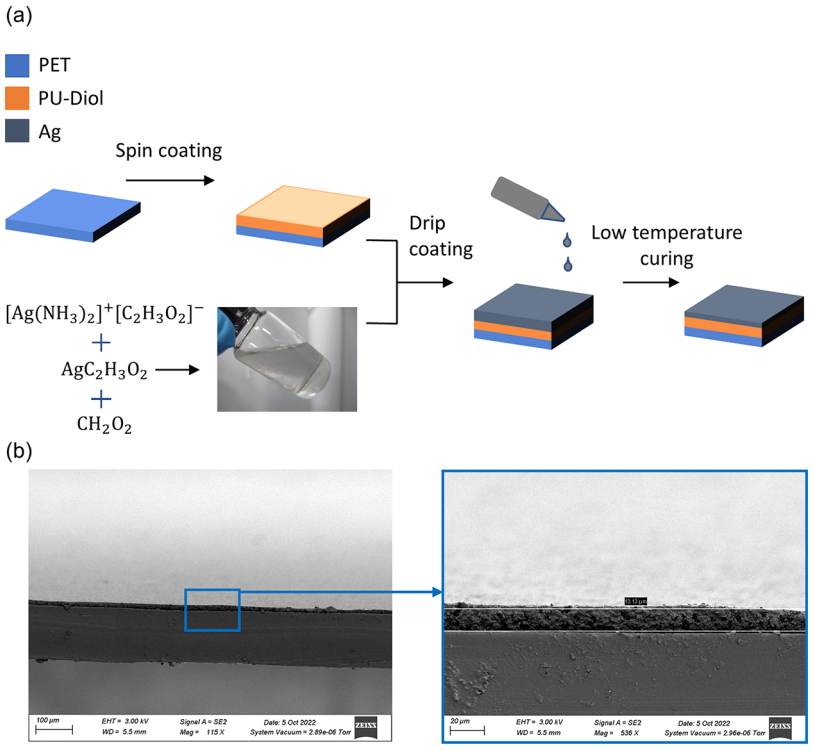

Figure 1. Schematic and characterization of Ag-PUD-PET. (a) Fabrication process flow for the Ag-PUD-PET. (b) SEM images of the cross section of Ag-PUD-PET.

an input of 4 V.[26] George et al. reported that single-wall carbon nanotubes could achieve 120 °C stable heating temperature with 1.5 V DC input.[27] Sun et al. reported that polyimide fiber (PIF)/MXene composites could reach 120 °C at 2.5 V DC input.[28] It has been difficult for researchers to achieve higher than 125 °C stable temperature using less than 2 V input as this requires very low resistance.

Different metal deposition methods have been demonstrated as useful approaches to fabricate metal thin films such as electroplating,[29] plasma induced reduction,[18] and sputter coating.[30] However, there are some shortcomings with these methods—they usually require vacuum or high energy to perform the deposition. Recent research in conductive inks[15,16,31] and additive manufacturing methods such as gravure, flexographic, offset, and inkjet printing have demonstrated the ability to print electronics on a variety of soft and flexible substrates, while reducing material and energy consumed.[32,33] These 3D printing technologies provide high throughput, lightweight, and roll-to-roll process integration.[34]

Herein, we demonstrate an ultrahigh conductance silver coating thin film on PET, where the as prepared conductive thin film shows higher than 80 dB EMI SE and 147 °C Joule heating at 1.5 V DC power input. The silver coating process only uses ambient pressure and low temperature curing (100 °C) and one time coating to achieve a thickness of 5.8 to 11.7 μm. The thickness can be controlled by varying the drip coating volume. The silver ink consists of a reactive silver ink, which can achieve high conductivities at low curing temperatures.[35] Coated samples with a thickness of 11.7 μm were observed to have sheet resistance as low as 56.9 mohm/sq and SE as high as 82.6 dB EMI in the X band (8−12 GHz) and 85.3 dB EMI in the Ku band (12−18 GHz). Without the PUD, the silver films crack after a single bend. Polyurethane diol (PUD) is utilized as a binding agent to enhance adhesion between the cured silver and the PET and enable repeated bending of the silver film. As prepared samples have good flexibility, and the sheet resistance does not have a significant change for 1.2 or 0.4 cm bending radius after 10 000 bending cycles and maintains high SE. The proposed coating method also shows great potential for Joule heating. The 11.7 μm thickness sample heats to 98.1 °C in 10 s and stabilizes at between 136 to 147 °C under only 1.5 V DC power. The coated metal thin films are demonstrated as a promising new material for flexible EMI shielding and Joule heating film which could be scalable fabricated on flexible plastics such as PET and may be used for applications such as smart wearables, medical electronics, and next generation communications.

RESULTS AND DISCUSSION

Figure 1 shows how the silver thin films were prepared on PET and their morphology. The process preparation is shown in Figure 1a. A thin layer of polyurethane diol (PUD) was spin coated onto cleaned PET to increase the adhesion of the silver to the PET. The carboxyl groups in the PUD strengthen adhesion by forming hydrogen bonds with the silver ink in the liquid phase as well as hydrogen bonds with the PET.[36] After that, Ag ink was drip coated on the PET with varying volumes. Ag ink coated samples were cured at 100 °C for 1 h in an oven. In this simple coating protocol, we avoid vacuum processes and high temperature curing as required in traditional Ag thin film deposition process. Thus, our process demonstrates a more convenient way to coat high quality Ag films on flexible substrates, such as polymers which are sensitive to high temperature processes. Figure 1b shows cross-sectional scanning electron microscope (SEM) images of 250 μL ink coated Ag films. The Ag coating is uniform from the side view over the PET. Figure S1 shows cross section SEM images of different thickness films coated from different volume Ag ink.

https://doi.org/10.1021/acsaelm.2c01183
ACS Appl. Electron. Mater. XXXX, XXX, XXX−XXX

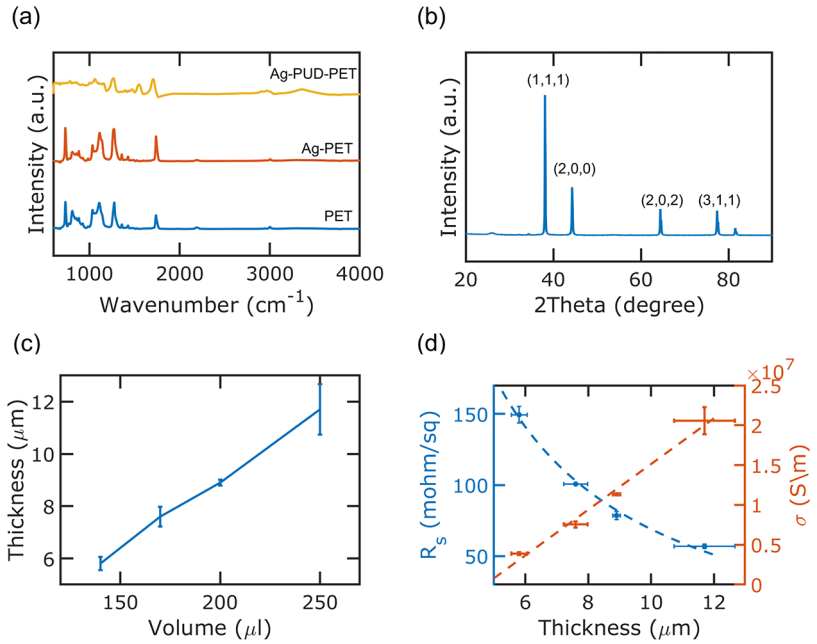

Figure 2. Chemical and structural characterization of cured Ag films. (a) FTIR for PET, Ag-PET, and Ag-PUD-PET, respectively, and (b) XRD for Ag-PUD-PET. (c) Thickness of Ag layer from SEM for different volume coated Ag-PUD-PET. (d) Sheet resistance and electric conductivity at different thicknesses.

Figure 2 shows the chemical and structure characterization of fabricated films. To evaluate the chemical composition, Fourier-transform infrared spectroscopy (FTIR) and X-ray diffraction (XRD) were used. In Figure 2a, FTIR results of the PET film, cured silver on PET (Ag-PET), and cured silver on PUD on PET (Ag-PUD-PET) are all shown. For the Ag-PUD-PET, the 1158 cm^{-1} C−N stretching peak, 1547 cm^{-1} N−H bending peak, 2960 cm^{-1} C−H stretching peak, and 3355 cm^{-1} N−H stretching peak validate the presence of PUD.[37,38] Figure 2b shows the XRD results of the Ag-PUD-PET. The narrow peaks at 2θ = 38.1, 44.3, 64.4, and 77.4° correspond to the (1, 1, 1), (2, 0, 0) (2, 0, 2), and (3, 1, 1) planes of Ag, respectively. Figure 2c shows the film thickness relation to the drip coating volume of the ink. Here, 2.5 cm × 2.5 cm PET films were coated with varying volumes of reactive silver ink. With increasing coating volume, the average Ag film thickness increase from 5.8 to 11.7 μm. Figure 2d shows the relationship between silver film thickness and sheet resistance, and film thickness and conductivity of the film. When the silver film thickness increase from 5.8 to 11.7 μm, the sheet resistance decreases from 148.7 to 56.9 mohm/sq, and the conductivity of as prepared Ag films increases from 3.9×10^6 to 2.0×10^7 S/m. The conductivity increases with increasing Ag film thickness as surface scattering has less influence on the overall conductivity of the film. Bulk Ag conductivity is 6.3×10^7 S/m, so the cured Ag films have conductivities ranging from 6.2% to 31.7% of bulk Ag.

The EMI SE performance of our Ag-PUD-PET samples were measured by the coaxial transmission line method. The shielding efficiency (SE) is defined on the logarithm scale,

$$\mathrm{SE} = -10 \log_{10} T \tag{1}$$

where T is the transmission coefficient of the sample.

Figure 3 shows the SE for Ag-PUD-PET at the frequency range of (a) 8−12 GHz and (b) 12−18 GHz for the four different thickness samples. The SE data has a jump at 12 GHz

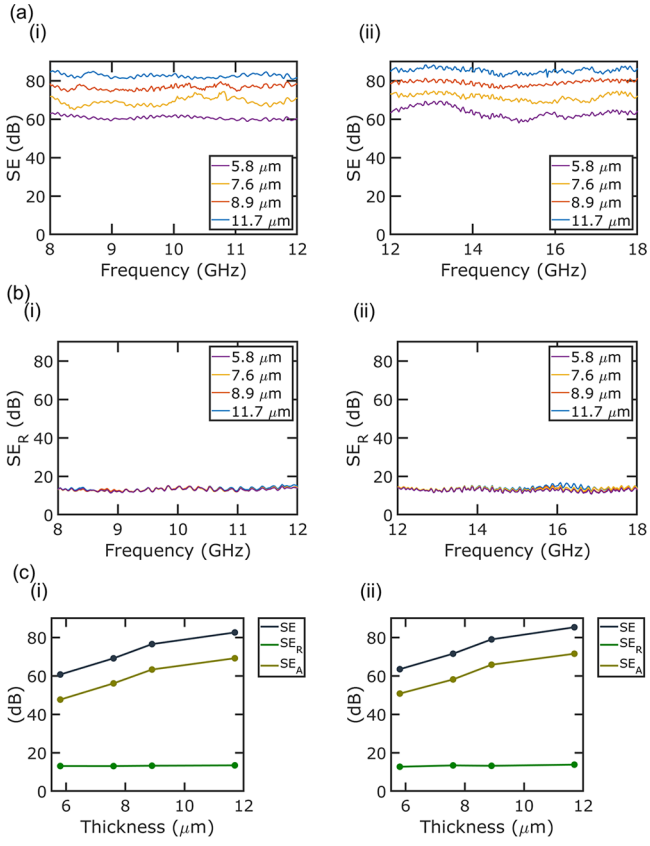

Figure 3. EMI shielding performance of varying thickness Ag-PUD-PET. (a) Ag-PUD-PET SE in the frequency range of (i) 8−12 GHz and (ii) 12−18 GHz for varying thickness films. (b) Ag-PUD-PET SE_R in the frequency range of (i) 8−12 GHz and (ii) 12−18 GHz. (c) Ag-PUD-PET average EMI SE, SE_R and SE_A in the frequency range of (i) 8−12 GHz and (ii) 12−18 GHz as a function of film thickness.

https://doi.org/10.1021/acsaelm.2c01183
ACS Appl. Electron. Mater. XXXX, XXX, XXX−XXX

since the waveguide flange is different in the two plots. The average SE in the frequency range of 8−12 GHz for the 5.6, 7.6, 8.9, and 11.7 μm thick films are 60.7, 69.2, 76.6, and 82.6 dB, respectively. The average SE in the frequency range of 12−18 GHz for the 5.6, 7.6, 8.9, and 11.7 μm samples are 63.5, 71.6, 79.0, 85.3 dB, respectively. The shielding efficiency is comprised of two components, $SE = SE_R + SE_A$, where SE_R is the component of the shielding efficiency due to reflection and SE_A is the part of the shielding that is due to attenuation. These two components are defined as follows:

$$SE_R = -10 \log_{10}(1 - R) \quad (2)$$

where R is the reflection coefficient, and

$$SE_A = -10 \log_{10} \frac{T}{(1 - R)} \quad (3)$$

Figure 3b shows SE_R for Ag-PUD-PET of different thicknesses at the frequency range of (i) 8−12 GHz and (ii) 12−18 GHz. Figure 3c shows the average SE, SE_R, and SE_A for varying thickness of Ag-PUD-PET films in the frequency range of (i) 8−12 GHz and (ii) 12−18 GHz. As the thickness of the sample varies from 5.6 to 11.7 μm, SE at 8−12 GHz increases from 60.7 to 82.6 dB and for 12−18 GHz, increases from 63.5 to 85.3 dB. SE_R stays approximately constant for varying thickness films. The increase of SE is due to an increase in SE_A as the thickness of the film increases. The absorption coefficient A and reflection coefficient R of the samples are calculated and displayed in Figure S4. The average coefficients for absorption and reflection are 0.05 and 0.95, respectively, and have little dependence on frequency or thickness. For non magnetic metal-based EMI shielding, SE is mostly due to attenuation of the electric field in the metal film or equivalently, high absorption.[39]

Figure 4 shows a comparison of our results to previous work in the literature for average SE over the X band. We show

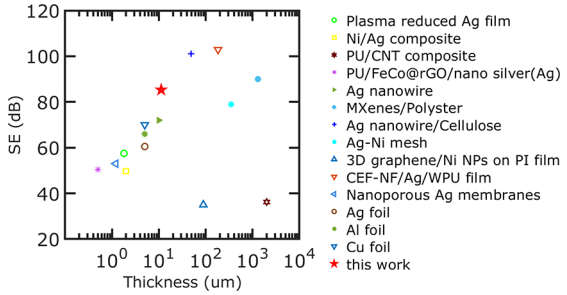

Figure 4. Comparison of EMI SE and thickness between our work to Plasma Ag deposition,[18] Ni/Ag composite,[14] PU/CNT composite,[40] PU/FeCo@rGO,[41] Ag nanowire,[11] MXenes/Polyester,[22] Ag nanowire/cellulose,[23] Ag−Ni mesh,[21] 3D graphene with Ni NPs,[21] CEF-NF/Ag/WPU film,[39] nanoporous Ag membranes,[42] Ag foil,[42] and Cu foil.[42]

results in the literature including plasma reduced Ag film,[18] Ni/Ag composites,[14] polyurethane/carbon nanotubes (PU/CNT) composites,[40] waterborne polyurethane composite film with FeCo alloy decoration and reduced graphene oxide (WPU/FeCo@rGO)/nano silver (Ag),[41] Ag nanowires,[11] MXene/polyester composite,[22] Ag nanowires with cellulose (Ag nanowire/cellulose),[23] Ag−Ni mesh,[21] 3D laser-induced graphene with nickel nanoparticles (Ni NPs) on polyimide (PI) substrate,[21] carbon-fabric/Ag/waterborne polyurethane film (CEF-NF/Ag/WPU film),[39] and Ag, Al, and Cu thin films.[42] In previous work, it has been difficult to achieve higher than 75 dB EMI SE with the thickness lower than 15 μm. For samples below 15 μm thick, Ag nanowires (right green triangle) were reported to achieve 72 dB SE at a thickness of 10 μm[11] and a Cu foil was reported to achieve 70 dB SE at the thickness of 5 μm. Achieving higher SE has required larger thicknesses. Ag nanowires with cellulose have been reported to achieve 101 dB with a thickness of 48.5 μm,[23] and a carbon-fabric/Ag/waterborne polyurethane film (CEF-NF/Ag/WPU film) was reported to achieve 102.9 dB at a thickness of 183 μm.[39] Our Ag-PUD-PET (highlighted with a red star) achieves over 80 dB SE at a thickness of only 11.7 μm.

Mechanical durability is important for the flexible electronics. Traditional metal deposition has the shortcoming of poor bending, adhesion, and twist durability. Ag-PET thin films without PUD were also fabricated. However, it was observed that the Ag film cracked after one bend and delaminated from the PET as shown in Figure S2. Due to the breakage, the film is not conductive, and the sheet resistance is infinite after just a single bend. The PUD is a binding agent that provides for better adhesion between the silver and the PET substrate, as described above. Optical pictures illustrating the flexibility of Ag-PUD-PET are shown in Figure S3. To evaluate the mechanical flexibility, we performed a series of bending, tape, and twist tests. Two bending radii were used in the experiments: 1.2 and 0.4 cm. Here, 10 000 bending cycles were executed for each bending radius, and the sheet resistance was measured after every 1000 bends. The metal film was on the outside of the PET during bending so that it is in a state of tension. We use the sheet resistance divided by the original sheet resistance (R_s/R_{s_o}) to describe change. For each bending radius, three sets of bending tests were implemented to get the standard error of R_s/R_{s_o}. The SE was recorded before and after 10 000 bends.

Figure S5 shows our bending results on a 1.2 cm radius cylinder and the results are discussed in the Supporting Information, where no statistically significant change in sheet resistance was observed. For the smaller bending radius of 0.4 cm as shown in Figure 5a(i), the two sample t test gives a p-value of 0.59, which supports the null hypothesis that R_s/R_{s_o} has no change after 10 000 bends. As prepared, Ag-PUD-PET films have good mechanical durability, and the sheet resistances have no statistically significant change after 10 000 bending cycles at a radii of 1.2 and 0.4 cm. The average EMI SE in the X band remains over 80 dB even after 10 000 bending cycles.

Parts a(ii) and a(iii) of Figure 5 show SE after 10 000 bends at a radius of 0.4 cm. Parts b and c of Figure 5 show the results for the Ag-PUD-PET films after 10 tape cycles and 1000 twist cycles, respectively. Tape cycle tests were performed with 3 M Scotch-brand tape, where each cycle consists of pressing tape onto the silver film and then peeling it off. Twist tests utilized 1.25 cm × 2.5 cm rectangular samples where the short dimension of the rectangular sample was twisted 180° with respect to the opposite side.[43] The Ag-PUD-PET films maintains its sheet resistance and SE after 10 tape cycles and 1,000 twist cycles, respectively, with no statistically significant change. The p-value for tape tests is 0.14 and for twisting is 0.46, which both support the null hypothesis of no change in R_s/R_{s_o} considering a significance level of $\alpha = 0.05$.

https://doi.org/10.1021/acsaelm.2c01183
ACS Appl. Electron. Mater. XXXX, XXX, XXX−XXX

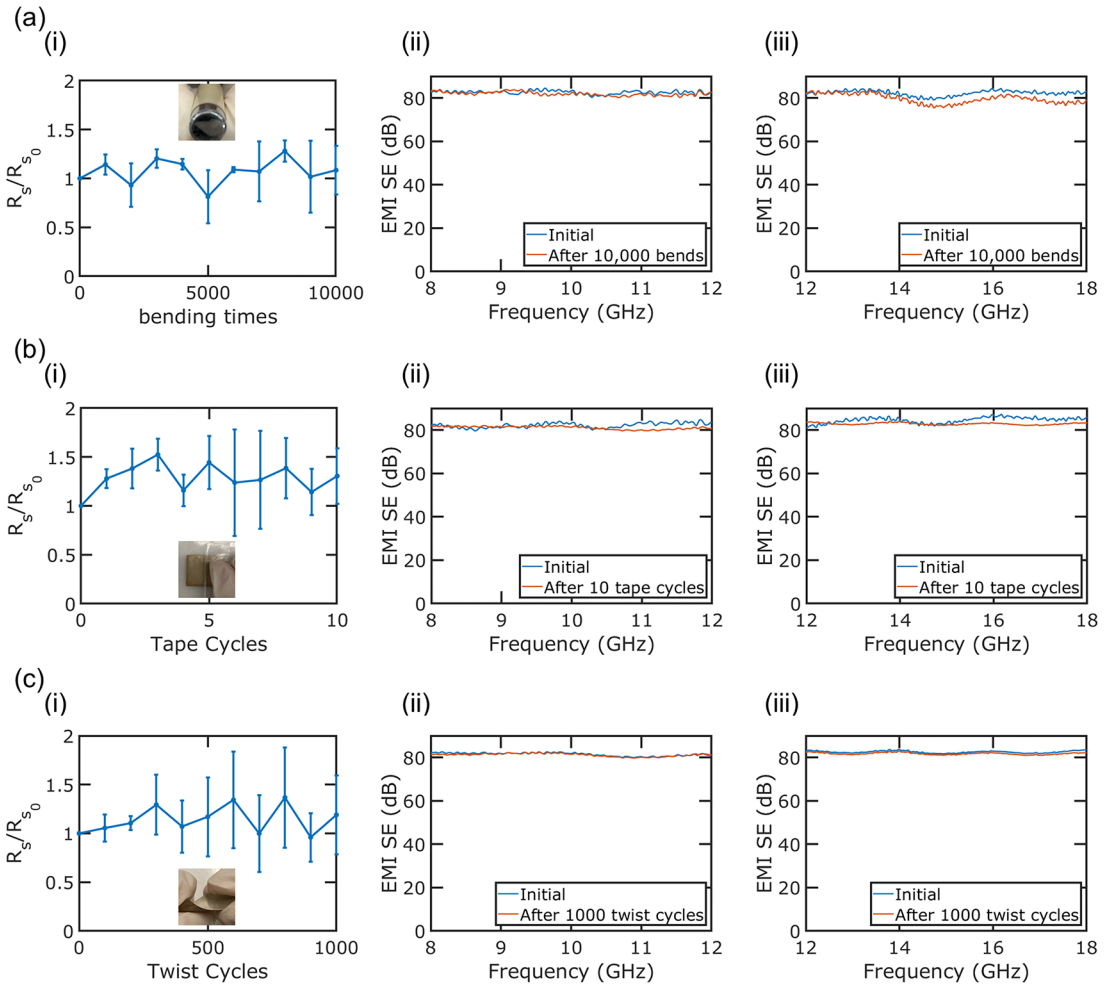

Figure 5. Sheet resistance of 11.7 μm coated Ag-PUD-PET divided by original sheet resistance during (a) 10 000 bending cycles at bending radius of 0.4 cm, (b) 10 taping cycles using 3 M Scotch tape, (c) and twisting test at twist angle of 180°. Comparison of EMI SE for untreated sample and treated sample after (a) bending, (b) taping, and (c) twisting at the frequency range of (ii) 8−12 GHz and (iii) 12−18 GHz.

When a voltage is applied to a conductor, electrons collide with phonons leading to the generation of heat. In the application of heat management devices, a lower input voltage is preferred for safety considerations, and thus lower resistances are needed. Figure 6a shows the voltage−current (U−I) curve of the as prepared 11.7 μm thick Ag-PUD-PET. To explore the voltage-controlled heating performance, we explore the stepwise heating and cooling as shown in Figure 6b. The 11.7 μm thick was tested with a voltage of 1.5 V at room temperature of 28.0 °C. In total, 5 voltage stages were applied on the sample, and each stage took 100 s. The Ag-PUD-PET has good heating efficiency even under low voltage because of its ultralow resistance, and the heating stable temperature could be controlled by the input voltage conveniently. Fast heating and cooling enables applications related to smart heat management device. Figure 6c shows the temperature mapping of the 11.7 μm coated sample under 1.5 V applied. For the first 10−30 s, the heat generation is mostly at the edges where the samples are connected to the metal clips. From 40 to 60 s, the heat generation gradually spreads over the square film. At a time of 60 s, the center temperature is 137.0 °C. Figure 6d shows the variation of the Ag-PUD-PET temperature with 1.5 V applied. Different thickness samples have different stable temperature, where larger thickness samples achieve higher temperatures due to lower sheet resistance. After the applied voltage is removed, samples cool quickly back to 35.0 to 40.0 °C within 60 s.

As mentioned previously, heat management at low voltages is important for safety considerations. In Figure 7, we compare the stable temperature at different voltages between previous work and our Ag-PUD-PET. It gas been difficult for researchers to find a joule heating material which could maintain stable temperature at higher than 120 °C with the input DC voltage lower than 2 V. In Figure 7, we show the results in the literature including MXene fabric,[44] Carbon scaffolds,[45] Ag nanowire,[11] MXene/polyester,[22] Ag nanowire/cellulose,[23] Ag nanowire (AgNW)/leather,[24] boron nitride nanosheets (BNNS)/aramid nanofibers (ANF) -Ag nanowire (AgNW)/aramid nanofibers (ANF),[26] carbon nanotube-(CNT)/cellulose aerogel,[25] single-wall CNTs on glass fiber,[27] cellulose MXene composite paper,[46] and a polyimide fiber (PIF)/MXene composite film.[28] BNNS/ANF-AgNW/ANF is reported to achieve 90.1 °C at 2 V, 148.7 °C at 3 V, and 175.4 °C at 4 V.[26] Single-wall CNTs on glass fiber have been reported to achieve 75 °C at 1 V and 120 °C at 1.5 V.[27] A PIF/MXene composite film has been reported to achieve 38 °C at 1 V, 75 °C at 1.8 V, and 120 °C at 2.5 V.[28] Our Ag-PUD-PET is able to achieve 147.0 °C stable temperature with only 1.5 V applied, due to the very low sheet resistance.

https://doi.org/10.1021/acsaelm.2c01183
ACS Appl. Electron. Mater. XXXX, XXX, XXX−XXX

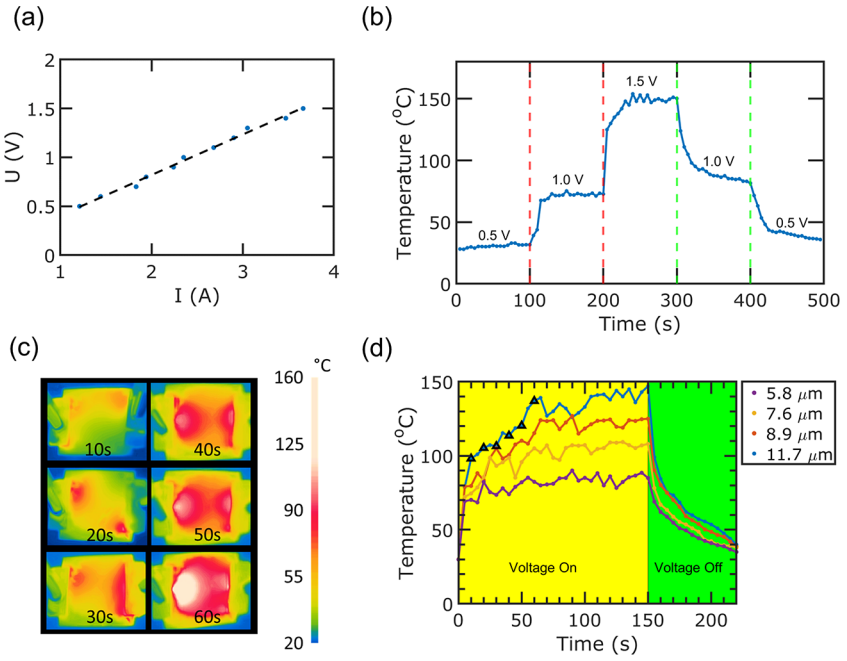

Figure 6. Joule heating performance of Ag-PUD-PET. (a) U−I curve for 11.7 μm coated sample using the DC voltage from 0.5−1.5 V. (b) Stepwise heating/cooling curve for 11.7 μm coated sample. (c) Temperature mapping from 10 to 60 s for the 11.7 μm coated sample at voltage of 1.5 V. (d) Joule heating/cooling curve for different volume coated samples under the voltage of 1.5 V.

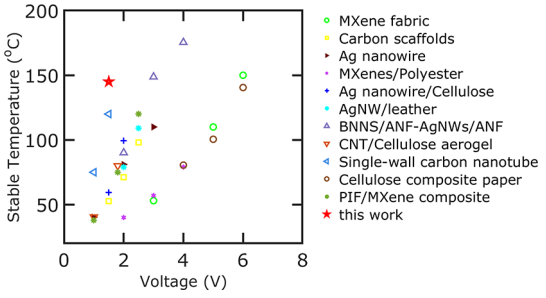

Figure 7. Comparison of Joule heating voltage/stable temperature or our Ag-PUD-PET with MXene fabric,[44] carbon scaffolds,[45] Ag nanowire,[11] MXenes/polyester,[22] Ag nanowire/cellulose,[23] AgNW/leather,[24] BNNS/ANF-AgNWs/ANF,[26] CNT/cellulose aerogel,[25] single-wall carbon nanotube,[27] cellulose composite paper,[46] and PIF/MXene composite.[28]

CONCLUSION

We report an ultrahigh conductance flexible Ag coating on PET substrate which exhibits excellent EMI shielding efficiency and Joule heating ability. We use drip coating volume to control the thickness of the film and evaluate the EMI SE and joule heating performance of as prepared samples. The resultant Ag-PUD-PET thin film exhibited an ultralow sheet resistance of 56.9 mohm/sq and EMI SE as high as 82.6 dB in X band (8−12 GHz) and 85.3 dB in Ku band (12−18 GHz). The shielding efficiency source was explored by calculating the contribution from the reflection and attenuation. It was observed that the increase the film thickness reduces the sheet resistance and increases the SE from attenuation, but it does not change the SE from the reflection. Because of the use of PUD to enhance adhesion, the Ag film exhibited a great flexibility, as prepared film sheet resistances do not have a statistically significant change after 10 000 bending cycles at 1.2 and 0.4 cm bending radii, 10 tape adhesion/peeling cycles, and 1000 twist cycles. The EMI SE remains higher than 80 dB in the X band after the bending tests. The excellent conductance enables high Joule heating performance for the Ag-PUD-PET thin films. We applied DC power on the sample and varied voltages. The as prepared sample has a stable temperature of 147.0 °C at an applied voltage of 1.5 V. The stepwise voltage temperature curve shows a good control ability of temperature by voltage. Our coating method demonstrates advantages of low material consumption and easy scalable processing. The as demonstrated material has great potential in communication industry, thermal management medical devices and multifunctional flexible smart electronics.

EXPERIMENTAL SECTION

Ink Information. Commercially available EI-710, a silver metal-complex based conductive ink from Electroninks Inc., was used in this study. The ink is based on ink previously developed by one of the authors[35] has a viscosity of 8 cps with a solid content of approximately 12%. In the ink, the ammonia ligands compounds is stabilizer. When the ink gets cured in an oven, the liable ammonia ligands compounds evaporate, and then the silver compound gets reduced to solid silver.

Fabrication of Silver Thin Film. ST505 PET (150 μm thick) was cut into 2.5 cm × 2.5 cm pieces and then rinsed in a 1:1 acetone:ethanol solution. Samples were ultrasonically agitated (Branson 5510 Ultrasonic Shaker) for 3 min and then rinsed with deionized water, and dried with nitrogen. Oxygen plasma treatment (Fischione Instruments Model 1070 NanoClean Plasma Cleaner) was used to make the PET surface hydrophilic. A polyurethane diol (PUD) layer was spin coated in 5 steps: (1) 8.9 rpm for 60 s, (2) 1000 rpm for 60 s, (3) 3000 rpm for 60 s, (4) 4000 rpm for 20 s, and (5) 10000 rpm for 60 s. After that, the EI-710 Ag ink was drip coated with a desired volume controlled by pipet. The Ag ink was cured in an oven (Quincy Lab Model 10 Lab Oven) at 100 °C for 1 h.

Characterization. The morphology and thickness were characterized using Zeiss SIGMA VP Scanning Electron Microscope. To avoid the surface charge on polymer layer, a Pd layer was deposited on the sample (Denton Sputter Coater) at current = 30 mA, time = 40 s. XRD diffraction of the Ag thin film was performed on the Bruker D8 Discover XRD system. FTIR was obtained using a Bruker

https://doi.org/10.1021/acsaelm.2c01183
ACS Appl. Electron. Mater. XXXX, XXX, XXX−XXX

VERTEX-70LS FTIR. Sheet resistance were measured from a four point probe (Keysight B1500A).

The EMI SE were obtained from a coaxial transmitted line method (HP 7822D vector network analyzer). Waveguide flanges (PASTERNACK) for X band (8−12 GHz) and Ku band (12−18 GHz) were used to measure the EMI SE. Samples were mounted between flanges and we used screws and nuts to keep the two flanges stable. DC power used in the Joule heating test utilized a NANKADF 30 V 10A Bench Power Supply. A FLIR ONE PRO IR camera was used to collect the IR image data for the joule heating.

Flexibility and Durability Characterization. Bending tests were performed by bending a 2.5 cm × 2.5 cm silver film with PUD on PET sample (Ag-PUD-PET) around a cylinder with radius 1.2 or 0.4 cm. Each bending cycle consists of bending the sample around the cylinder and then unbending the sample to a flat configuration.

Tape tests were performed with 3 M Scotch-brand tape on a 2.5 cm × 2.5 cm Ag-PUD-PET sample. Each tape cycle consists of sticking the tape onto the silver film and then peeling off the tape.

Twist tests were performed on sample size of 1.25 cm × 2.5 cm. For each twist cycle, the short dimension of the rectangular sample (1.25 cm) was twisted 180° with respect to the opposite side of the same sample. The twisting angle definition is the same as that used in other literature with regards to twist tests.[43,47]

■ ASSOCIATED CONTENT

Supporting Information

The Supporting Information is available free of charge at https://pubs.acs.org/doi/10.1021/acsaelm.2c01183.

SEM of Ag-PUD-PET, optical images of Ag-PET, optical images of Ag-PUD-PET, power coefficients of Ag-PUD-PET, and bending test for Ag-PUD-PET (PDF)

■ AUTHOR INFORMATION

Corresponding Author

Paul W. Leu − *Department of Industrial Engineering and Department of Mechanical Engineering, University of Pittsburgh, Pittsburgh, Pennsylvania 15261, United States; Department of Chemical Engineering, University of Pittsburgh, Pittsburgh, Pennsylvania 15261, United States;* Email: pleu@pitt.edu

Authors

Mingxuan Li − *Department of Chemical Engineering, University of Pittsburgh, Pittsburgh, Pennsylvania 15261, United States;* orcid.org/0000-0001-6217-9382

Sneh Sinha − *Electroninks Incorporated, Austin, Texas 78744, United States*

Sima Hannani − *Electroninks Incorporated, Austin, Texas 78744, United States*

S. Brett Walker − *Electroninks Incorporated, Austin, Texas 78744, United States*

Melbs LeMieux − *Electroninks Incorporated, Austin, Texas 78744, United States*

Complete contact information is available at: https://pubs.acs.org/10.1021/acsaelm.2c01183

Notes

The authors declare no competing financial interest.

■ ACKNOWLEDGMENTS

The authors acknowledge support from the MDS-Rely Center to conduct this research. The MDS-Rely Center is supported by the National Science Foundations IndustryUniversity Cooperative Research Center (IUCRC) Program under Awards EEC-2052662 and EEC-2052776.

■ REFERENCES

(1) Geetha, S.; Satheesh Kumar, K. K.; Rao, C. R. K.; Vijayan, M.; Trivedi, D. C. EMI shielding: Methods and materials—A review. *J. Appl. Polym. Sci.* **2009**, *112*, 2073−2086.

(2) Bhattacharjee, Y.; Bose, S. Core−Shell Nanomaterials for Microwave Absorption and Electromagnetic Interference Shielding: A Review. *ACS Appl. Nano Mater.* **2021**, *4*, 949−972.

(3) Ozdemir, F.; Kargi, A. In *Electromagnetic Waves*. Zhurbenko, V., Ed.; IntechOpen: Rijeka, Croatia, 2011; Chapter 22.

(4) Kuhn, M. G.; Anderson, R. J.*Soft Tempest: Hidden Data Transmission Using Electromagnetic Emanations*; Information Hiding: Berlin and Heidelberg, Germany, 1998; pp 124−142.

(5) van Eck, W. Electromagnetic radiation from video display units: An eavesdropping risk? *Computers & Security* **1985**, *4*, 269−286.

(6) Bohl, J.; Stark, R.; Wollman, G.RF-weapons for non lethal interference and destruction of communication, information and electronic systems. *Proceedings of the 3rd European Symposium on Non-Lethal Weapons, Ettlingen, Germany 10-12 May 2005*; 2005.

(7) Pereira, V.; Kunkolienkar, G. R. EMP (Electro-Magnetic Pulse) weapon technology along with EMP shielding & detection methodology. *2013 Fourth International Conference on Computing, Communications and Networking Technologies (ICCCNT)* **2013**, 1−5.

(8) Wen, B.; Cao, M.; Lu, M.; Cao, W.; Shi, H.; Liu, J.; Wang, X.; Jin, H.; Fang, X.; Wang, W.; Yuan, J. Reduced Graphene Oxides: Light-Weight and High-Efficiency Electromagnetic Interference Shielding at Elevated Temperatures. *Adv. Mater.* **2014**, *26*, 3484−3489.

(9) Liang, J.; Wang, Y.; Huang, Y.; Ma, Y.; Liu, Z.; Cai, J.; Zhang, C.; Gao, H.; Chen, Y. Electromagnetic interference shielding of graphene/epoxy composites. *Carbon* **2009**, *47*, 922−925.

(10) Geetha, S.; Satheesh Kumar, K. K.; Rao, C. R. K.; Vijayan, M.; Trivedi, D. C. EMI shielding: Methods and materials—A review. *J. Appl. Polym. Sci.* **2009**, *112*, 2073−2086.

(11) Wang, Y.; Peng, S.; Zhu, S.; Wang, Y.; Qiang, Z.; Ye, C.; Liao, Y.; Zhu, M. Biomass-Derived, Highly Conductive Aqueous Inks for Superior Electromagnetic Interference Shielding, Joule Heating, and Strain Sensing. *ACS Appl. Mater. Interfaces* **2021**, *13*, 57930−57942.

(12) Blakey-Milner, B.; Gradl, P.; Snedden, G.; Brooks, M.; Pitot, J.; Lopez, E.; Leary, M.; Berto, F.; du Plessis, A. Metal additive manufacturing in aerospace: A review. *Materials & Design* **2021**, *209*, 110008.

(13) Abdulhameed, O.; Al-Ahmari, A.; Ameen, W.; Mian, S. H. Additive manufacturing: Challenges, trends, and applications. *Advances in Mechanical Engineering* **2019**, *11*, 168781401882288.

(14) Liu, X.; Ye, Z.; Zhang, L.; Feng, P.; Shao, J.; Zhong, M.; Chen, Z.; Ci, L.; He, P.; Ji, H.; Wei, J.; Li, M.; Zhao, W. Highly flexible electromagnetic interference shielding films based on ultrathin Ni/Ag composites on paper substrates. *J. Mater. Sci.* **2021**, *56*, 5570−5580.

(15) Galante, A. J.; Li, M.; Pilsbury, B.; LeMieux, M.; Liu, Q.; Leu, P. W. Achieving Highly Conductive, Stretchable, and Washable Fabric from Reactive Silver Ink and Increased Interfacial Adhesion. *ACS Appl. Polym. Mater.* **2022**, *4*, 5253.

(16) Galante, A. J.; Yates, K. A.; Pilsbury, B.; LeMieux, M.; Bain, D. J.; Romanowski, E. G.; Shanks, R. M. Q.; Leu, P. W. Reactive silver inks for antiviral, repellent medical textiles with ultrasonic bleach washing durability compared to silver nanoparticles'. *PLoS One* **2022**, *17*, e0270718.

(17) Tomioka, Y.; Yuki, N. Bend stiffness of copper and copper alloy foils. *Journal of Materials Processing Technology* **2004**, *146*, 228−233.

(18) Oh, H.-J.; Dao, V.-D.; Choi, H.-S. Electromagnetic shielding effectiveness of a thin silver layer deposited onto PET film via atmospheric pressure plasma reduction. *Appl. Surf. Sci.* **2018**, *435*, 7−15.

(19) Rao, M. S.EMI/EMC effects on EW receiver systems of Military aircraft. 2008 10th International Conference on Electro-

magnetic Interference & Compatibility. *10th International Conference on Electromagnetic Interference & Compatibility*; 2008; pp 63−67.
(20) Kamchi, N. E.; Belaabed, B.; Wojkiewicz, J.-L.; Lamouri, S.; Lasri, T. Hybrid polyaniline/nanomagnetic particles composites: High performance materials for EMI shielding. *J. Appl. Polym. Sci.* **2013**, *127*, 4426−4432.
(21) Yin, J.; Zhang, J.; Zhang, S.; Liu, C.; Yu, X.; Chen, L.; Song, Y.; Han, S.; Xi, M.; Zhang, C.; Li, N.; Wang, Z. Flexible 3D porous graphene film decorated with nickel nanoparticles for absorption-dominated electromagnetic interference shielding. *Chem. Eng. J.* **2021**, *421*, 129763.
(22) Wang, Q.-W.; Zhang, H.-B.; Liu, J.; Zhao, S.; Xie, X.; Liu, L.; Yang, R.; Koratkar, N.; Yu, Z.-Z. Multifunctional and Water-Resistant MXene-Decorated Polyester Textiles with Outstanding Electromagnetic Interference Shielding and Joule Heating Performances. *Adv. Funct. Mater.* **2019**, *29*, 1806819.
(23) Liang, C.; Ruan, K.; Zhang, Y.; Gu, J. Multifunctional Flexible Electromagnetic Interference Shielding Silver Nanowires/Cellulose Films with Excellent Thermal Management and Joule Heating Performances. *ACS Appl. Mater. Interfaces* **2020**, *12*, 18023−18031.
(24) Ma, Z.; Xiang, X.; Shao, L.; Zhang, Y.; Gu, J. Multifunctional Wearable Silver Nanowire Decorated Leather Nanocomposites for Joule Heating, Electromagnetic Interference Shielding and Piezoresistive Sensing. *Angew. Chem., Int. Ed.* **2022**, *61*, e202200705.
(25) Guo, Z.; Sun, C.; Wang, J.; Cai, Z.; Ge, F. High-Performance Laminated Fabric with Enhanced Photothermal Conversion and Joule Heating Effect for Personal Thermal Management. *ACS Appl. Mater. Interfaces* **2021**, *13*, 8851−8862.
(26) Han, Y.; Ruan, K.; Gu, J. Janus (BNNS/ANF)-(AgNWs/ANF) thermal conductivity composite films with superior electromagnetic interference shielding and Joule heating performances. *Nano Research* **2022**, *15*, 4747−4755.
(27) Karalis, G.; Tzounis, L.; Dimos, E.; Mytafides, C. K.; Liebscher, M.; Karydis-Messinis, A.; Zafeiropoulos, N. E.; Paipetis, A. S. Printed Single-Wall Carbon Nanotube-Based Joule Heating Devices Integrated as Functional Laminae in Advanced Composites. *ACS Appl. Mater. Interfaces* **2021**, *13*, 39880−39893.
(28) Sun, K.; Wang, F.; Yang, W.; Liu, H.; Pan, C.; Guo, Z.; Liu, C.; Shen, C. Flexible Conductive Polyimide Fiber/MXene Composite Film for Electromagnetic Interference Shielding and Joule Heating with Excellent Harsh Environment Tolerance. *ACS Appl. Mater. Interfaces* **2021**, *13*, 50368−50380.
(29) Ohiri, K. A.; Nowicki, N. M.; Montalbano, T. J.; Presley, M.; Lazarus, N. S. Electroplating of Aerosol Jet-Printed Silver Inks. *Adv. Eng. Mater.* **2021**, *23*, 2100362.
(30) Wang, H.; Ji, C.; Zhang, C.; Zhang, Y.; Zhang, Z.; Lu, Z.; Tan, J.; Guo, L. J. Highly Transparent and Broadband Electromagnetic Interference Shielding Based on Ultrathin Doped Ag and Conducting Oxides Hybrid Film Structures. *ACS Appl. Mater. Interfaces* **2019**, *11*, 11782−11791.
(31) Walker, S. B.; Lewis, J. A. Reactive Silver Inks for Patterning High-Conductivity Features at Mild Temperatures. *J. Am. Chem. Soc.* **2012**, *134*, 1419−1421.
(32) Li, J.; Wang, Y.; Xiang, G.; Liu, H.; He, J. Hybrid Additive Manufacturing Method for Selective Plating of Freeform Circuitry on 3D Printed Plastic Structure. *Advanced Materials Technologies* **2019**, *4*, 1800529.
(33) Zhou, Z.; Walker, S. B.; LeMieux, M.; Leu, P. W. Polymer-Embedded Silver Microgrids by Particle-Free Reactive Inks for Flexible High-Performance Transparent Conducting Electrodes. *ACS Appl. Electron. Mater.* **2021**, *3*, 2079−2086.
(34) Singh, M.; Haring, A. P.; Tong, Y.; Cesewski, E.; Ball, E.; Jasper, R.; Davis, E. M.; Johnson, B. N. Additive Manufacturing of Mechanically Isotropic Thin Films and Membranes via Microextrusion 3D Printing of Polymer Solutions. *ACS Appl. Mater. Interfaces* **2019**, *11*, 6652−6661.
(35) Walker, S. B.; Lewis, J. A. Reactive Silver Inks for Patterning High-Conductivity Features at Mild Temperatures. *J. Am. Chem. Soc.* **2012**, *134*, 1419−1421.
(36) Swapna, V.; Stephen, R.*Polyhedral Oligomeric Silsesquioxane (POSS) Polymer Nanocomposites*; Elsevier: 2021; pp 385−403.
(37) Mouzakis, D.; Papatzani, S.*Eco-Friendly Waterborne Polyurethanes*; CRC Press: 2022; pp 213−229.
(38) Suhasini, A.; Kumar, K. V.; Maiyalagan, T. Synthesis, thermal and magnetic behavior of iron oxide-polymer nanocomposites. *Science and Engineering of Composite Materials* **2018**, *25*, 189−195.
(39) Xing, D.; Lu, L.; Xie, Y.; Tang, Y.; Teh, K. S. Highly flexible and ultra-thin carbonfabric/ Ag/waterborne polyurethane film for ultra-efficient EMI shielding. *Materials & Design* **2020**, *185*, 108227.
(40) Feng, D.; Xu, D.; Wang, Q.; Liu, P. J. Highly stretchable electromagnetic interference (EMI) shielding segregated polyurethane/carbon nanotube composites fabricated by microwave selective sintering. *J. Mater. Chem. C* **2019**, *7*, 7938−7946.
(41) Zhu, H.; Yang, Y.; Sheng, A.; Duan, H.; Zhao, G.; Liu, Y. Layered structural design of flexible waterborne polyurethane conductive film for excellent electromagnetic interference shielding and low microwave reflectivity. *Appl. Surf. Sci.* **2019**, *469*, 1−9.
(42) Lim, G.-H.; Kwon, N.; Han, E.; Bok, S.; Lee, S.-E.; Lim, B. Flexible Nanoporous Silver Membranes with Unprecedented High Effectiveness for Electromagnetic Interference Shielding. *Journal of Industrial and Engineering Chemistry* **2021**, *93*, 245−252.
(43) Jia, L.-C.; Yan, D.-X.; Yang, Y.; Zhou, D.; Cui, C.-H.; Bianco, E.; Lou, J.; Vajtai, R.; Li, B.; Ajayan, P. M.; Li, Z.-M. High strain tolerant EMI shielding using carbon nanotube network stabilized rubber composite. *Advanced Materials Technologies* **2017**, *2*, 1700078.
(44) Zhang, X.; Wang, X.; Lei, Z.; Wang, L.; Tian, M.; Zhu, S.; Xiao, H.; Tang, X.; Qu, L. Flexible MXene-Decorated Fabric with Interwoven Conductive Networks for Integrated Joule Heating, Electromagnetic Interference Shielding, and Strain Sensing Performances. *ACS Appl. Mater. Interfaces* **2020**, *12*, 14459−14467.
(45) Zhao, B.; Bai, P.; Wang, S.; Ji, H.; Fan, B.; Zhang, R.; Che, R. High-Performance Joule Heating and Electromagnetic Shielding Properties of Anisotropic Carbon Scaffolds. *ACS Appl. Mater. Interfaces* **2021**, *13*, 29101−29112.
(46) Li, E.; Pan, Y.; Wang, C.; Liu, C.; Shen, C.; Pan, C.; Liu, X. Multifunctional and superhydrophobic cellulose composite paper for electromagnetic shielding, hydraulic triboelectric nanogenerator and Joule heating applications. *Chem. Eng. J.* **2021**, *420*, 129864.
(47) Hong, S.; Yoo, S. S.; Lee, J. Y.; Yoo, P. J. Sonochemically activated synthesis of gradationally complexed Ag/TEMPO-oxidized cellulose for multifunctional textiles with high electrical conductivity, super-hydrophobicity, and efficient EMI shielding. *Journal of Materials Chemistry C* **2020**, *8*, 13990−13998.

https://doi.org/10.1021/acsaelm.2c01183
ACS Appl. Electron. Mater. XXXX, XXX, XXX−XXX